

Premelting controlled active matter in ice

Jérémy Vachier^{1,*} and John S. Wettlaufer^{1,2,†}

¹*Nordita, KTH Royal Institute of Technology and Stockholm University,
Hannes Alfvéns väg 12, SE-106 91 Stockholm, Sweden*

²*Yale University, New Haven, Connecticut 06520-8109, USA*

(Dated: October 20, 2021)

Self-propelled particles can undergo complex dynamics due to a range of bulk and surface interactions. When a particle is embedded in a host solid near its bulk melting temperature, the latter may melt at the surface of the former in a process known as interfacial premelting. The thickness of the melt film depends on the temperature, impurities, material properties and geometry. A temperature gradient is accompanied by a thermomolecular pressure gradient that drives the interfacial liquid from high to low temperatures and hence the particle from low to high temperatures, in a process called thermal regelation. When the host material is ice and the embedded particle is a biological entity, one has a particularly novel form of active matter, which addresses interplay between a wide range of problems, from extremophiles of both terrestrial and exobiological relevance to ecological dynamics in Earth's cryosphere. Of basic importance in all such settings is the combined influence of biological activity and thermal regelation in controlling the redistribution of bioparticles. Therefore, we re-cast this class of regelation phenomena in the stochastic framework of active Ornstein-Uhlenbeck dynamics and make predictions relevant to this and related problems of interest in biological and geophysical problems. We examine how thermal regelation compromises paleoclimate studies in the context of ice core dating and we find that the activity influences particle dynamics during thermal regelation by enhancing the effective diffusion coefficient. Therefore, accurate dating relies on a quantitative treatment of both effects.

I. INTRODUCTION

Glaciers, ice sheets, sea ice and permafrost constitute large ecosystems and cover significant areas of the planet [1–4]. Ice cores provide the highest resolution records of paleoclimate for the last eight glacial cycles [5, 6]. Therefore, ice core dating methods are of primary importance in quantifying climate processes and providing empirical constraints for models used to predict future climates. Moreover, a multitude of biota are present in the cryosphere, from algae, such as *Chlamydomonas nivalis* or *Euglena viridis*, to diatoms [1, 3, 7] and bacteria, such as *Pseudomonas priestleyi* or *Pseudomonas syringae* [1, 2]. Through physical and/or chemical interactions, these micro-organisms interact with their surroundings thereby creating environmental feedback [1, 2]. An important property of most of these micro-organisms is their motility [4, 8, 9] and they commonly evolve and hence self-propel adjacent to ice-water interfaces. For example, *Williamson et al.* [10] and *Ryan et al.* [11] have recently shown that biota can accelerate the melting of ice in Greenland. Moreover, studies of sea ice support the idea that the migration of a range of bacteria, eukaryotes and prokaryotes within the ice column are accompanied by phase change. In consequence a symbiotic relationship between sea ice biota and phase change is observed [12–14]. In contrast, the bacteria *Pseudomonas syringae* acts as a heterogeneous ice nucleus, and is used to create artificial snow [2]. Finally, the setting we study is of im-

portance in understanding extremophiles. For example, it has been shown that the evolution of microbial cells can be linked to permafrost age [3], a *living* Bdelloid rotifer has recently been recovered from permafrost 24,000 years old [15], and a new species has been discovered in 16 million-year-old amber [16]. Therefore, understanding the physico-chemical relationship between microorganisms and their environment underlies key questions concerning the covariation of life and climate.

Active particles are able to convert energy from biological, chemical, or physical processes into motion, and can exhibit macroscopic behavior that can lead to the emergence of collective motion [e.g., 17, 18]. Due the wide range of implications of their dynamics and their role as a model system in non-equilibrium statistical mechanics, active particles have been the focus of a great deal of attention in the past several decades [e.g., 9, 19–22]. Generally, active particles evolve in an aqueous environment where, because of their microscopic size, viscous forces dominate over inertial forces. Biological active particles, such as algae and bacteria, operate in complex geometries, for example in membranes, glaciers and ice sheets, and can react to chemical, physical and biological gradients, most commonly associated with nutrients and waste [23–25]. In the dilute case, where the particle-particle interactions can be neglected, the dynamics is dominated by the balance of active motion and external forces, such as gravity [26–29] or temperature gradients.

When a particle is embedded in ice near its bulk melting temperature, the ice may melt at the particle-ice surface in a process known as *interfacial premelting*. The thickness of the melt film depends on temperature, impurities, material properties and geometry [30]. A tem-

* jeremy.vachier@su.se

† john.wettlaufer@yale.edu

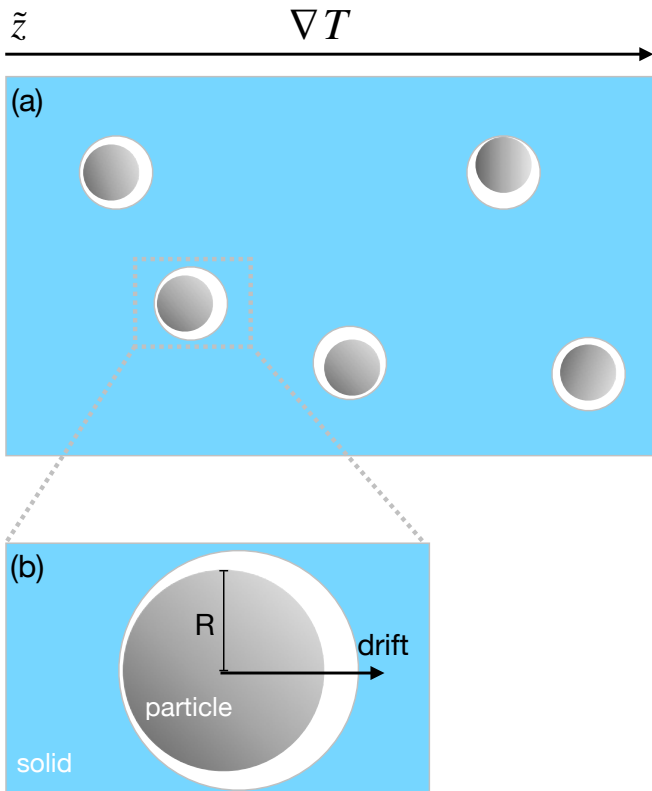


FIG. 1. (a) Perspective view of few active particles embedded inside a solid against which they premelt and experience an external temperature gradient ∇T . (b) An expanded view of one active particle inside the solid. The radius of the particle is R , the black arrow shows the drift velocity induced by thermal regelation.

perature gradient is accompanied by a thermomolecular pressure gradient that drives the interfacial liquid from high to low temperatures and hence the particle from low to high temperatures, in a process called *thermal regelation* [30–34].

Thermal regelation of inert particles plays a major role in the redistribution of material inside of ice, which has important environmental and composite materials implications [30–35]. However, surface properties are not only central to the physical processes shaping Arctic [36] and Antarctic [37] landscapes, but they underlie the fact that extremophile organisms on Earth develop strategies to act back on their harsh environments in order to improve living conditions. Important examples include expolymeric substance and antifreeze glycoproteins, both of which have unique impacts on the surface of ice that enhance liquidity [38]. The confluence of thermal regelation, bio-enhanced premelting and intrinsic mobility motivate the work described here.

The case of active particles in premelting solids as illustrated in Fig. 1. The fact that intrinsic mobility may compete with thermal regelation has not been previously studied, and is particularly relevant for biota in ice. For example, one known effect of the activity on a particle’s

dynamics is to change its diffusion properties [9]. Treating this question is particularly relevant for ice core paleoclimate dating methods due to the long periods of time over which diffusion can act [6, 39–41].

The framework of our study is that of a so-called active Ornstein-Uhlenbeck particle (AOUP) [e.g 42–48]. Here, the active force can vary and is represented by an “active diffusivity”, \tilde{D}_a , which is associated with a force that can be compared to a colored noise process [45, 49]. The AOUP possesses a characteristic time, τ_a , defining the noise persistence, which is the time scale after which the system switches from a ballistic to a diffusive regime. Both of these two key parameters, τ_a and \tilde{D}_a , can be measured experimentally [50–53].

The AOUP describes the motion of colloids in a bath of active particles [9, 50, 51] and, in the case of a bacterial bath, *Wu and Libchaber* [54] showed that the activity of the bacteria enhanced the diffusion of passive tracer particles by two to three orders of magnitude relative to the thermal case. Finally, while the AOUP model provides accurate predictions for a range of complex phenomena [44, 46, 47, 55], in contrast to the so-called Active Brownian Particle (ABP) and Run-and-Tumble models, a theoretical advantage of the AOUP is its Gaussian nature [45]. Moreover, similar to the ABP, the long term behavior of the AOUP is also diffusive [47]. These issues motivate our use of the AOUP model framework to describe the motion of active particles in ice under an external temperature gradient. We analyze these particles in three dimensions using a multiple scale expansion to derive the associated Fokker-Planck equation. Similar approaches have been used in the case of a passive Brownian particle [56–58] and for an active Brownian particle in a channel [59].

Our paper is organized as follows. In §II we outline the active Ornstein-Uhlenbeck particle model. In §III we derive the associated Fokker-Planck equation using a multiple scale expansion and then find the analytic solution in the limit that regelation dominates the dynamics. We then compare our analytic solutions with numerical solutions before concluding in §IV.

II. METHOD

As shown in Fig. 1, due to thermal regelation, the motion of the active particle is biased by a drift velocity $\tilde{v}(\tilde{z}) = U(\tilde{z})\hat{\tilde{z}}$ in the direction of the temperature gradient [34]. Regelation is a consequence of the premelted film around the particle, which can also execute diffusive motion in the ice column. The premelting-controlled diffusivity of the particle is given by $\tilde{D}(\tilde{z})\mathbb{I}$, where \mathbb{I} is the identity matrix [34]. The evolution of the particle’s position, $\tilde{\mathbf{r}} = (\tilde{r}_1, \tilde{r}_2, \tilde{r}_3) = (\tilde{x}, \tilde{y}, \tilde{z})$, and its activity are

described by two overdamped Langevin equations

$$\frac{d}{dt}\tilde{\mathbf{r}}(\tilde{t}) = \sqrt{2\tilde{D}_a}\tilde{\boldsymbol{\eta}}(\tilde{t}) + \tilde{v}(\tilde{z}) + \sqrt{2\tilde{D}(\tilde{z})}\boldsymbol{\xi}_p(\tilde{t}), \quad (1)$$

$$\frac{d}{dt}\tilde{\boldsymbol{\eta}}(\tilde{t}) = -\frac{1}{\tau_a}\tilde{\boldsymbol{\eta}}(\tilde{t}) + \frac{1}{\tau_a}\boldsymbol{\xi}_a(\tilde{t}). \quad (2)$$

The activity, or self-propulsion, is given by the term $\sqrt{2\tilde{D}_a}\tilde{\boldsymbol{\eta}}$ in Eq. (1), where \tilde{D}_a is the active diffusivity representing the active fluctuations of the system, which result from the interactions between tracer particles and their surrounding environment. Interesting examples include, among others, coupling to a viscoelastic medium, such as a cytoskeleton, or a bacterial bath [60–63].

The function $\tilde{\boldsymbol{\eta}} = (\tilde{\eta}_1, \tilde{\eta}_2, \tilde{\eta}_3)$ is described by an Ornstein-Uhlenbeck process, with correlations given by

$$\langle \tilde{\eta}_i(\tilde{t}')\tilde{\eta}_j(\tilde{t}) \rangle = \frac{\delta_{ij}}{\tau_a} e^{-\frac{|\tilde{t}'-\tilde{t}|}{\tau_a}}, \quad (3)$$

where τ_a is the noise persistence. In the small τ_a limit, $\tilde{\boldsymbol{\eta}}$ reduces to Gaussian white noise with correlations $\langle \tilde{\eta}_i(\tilde{t}')\tilde{\eta}_j(\tilde{t}) \rangle = \delta_{ij}\delta(\tilde{t}'-\tilde{t})$. In contrast, when τ_a is finite, $\tilde{\boldsymbol{\eta}}$ does not reduce to Gaussian white noise, and Eq. (1) does not reach equilibrium. Hence, τ_a controls the non-equilibrium properties of the system. The random fluctuations are given by zero mean Gaussian white noise processes $\langle \xi_{p_i}(\tilde{t}')\xi_{p_j}(\tilde{t}) \rangle = \delta_{ij}\delta(\tilde{t}'-\tilde{t})$ and $\langle \xi_{a_i}(\tilde{t}')\xi_{a_j}(\tilde{t}) \rangle = \delta_{ij}\delta(\tilde{t}'-\tilde{t})$. In the limit where soluble impurities control the premelted film thickness in ice, the velocity and diffusivity are given by

$$U(\tilde{z}) = -\frac{A_3}{A_2^3} \frac{1}{\tilde{z}^3}, \quad (4)$$

and

$$\tilde{D}(\tilde{z}) = \frac{(R_g T_m N_i)^3 k_B T_m}{8\pi\nu R^4 A_2^3} \frac{1}{\tilde{z}^3}, \quad (5)$$

with $A_2 = \rho_l q_m \frac{|\nabla T|}{T_m}$ and $A_3 = \rho_s q_m |\nabla T| \frac{(R_g T_m N_i)^3}{6\nu R T_m}$ [34]. The universal gas constant is R_g ; the latent heat of fusion per mole of the solid is q_m ; the molar density of the liquid is ρ_l ; the magnitude of the external temperature gradient is $|\nabla T|$; the pure bulk melting temperature is $T_m = 273.15\text{K}$; the viscosity of the fluid is ν ; the particle radius is R ; the number of moles of impurities per unit area of the interface is N_i ; k_B is Boltzmann's constant; and $\rho_s q_m \sim 334 \times 10^6 \text{ J}\cdot\text{m}^{-3}$ [34].

The Langevin Eqs. (1) and (2), allow us to express the probability of finding a particle at the position $\tilde{\mathbf{r}} = (\tilde{r}_1, \tilde{r}_2, \tilde{r}_3) = (\tilde{x}, \tilde{y}, \tilde{z})$ at a given time \tilde{t} through the Fokker-Planck equation, which describes the evolution of the probability density function $P(\tilde{\mathbf{r}}, \tilde{\boldsymbol{\eta}}, \tilde{t}|\tilde{\mathbf{r}}_0, \tilde{\boldsymbol{\eta}}_0, \tilde{t}_0)$, with the initial condition $P(\tilde{\mathbf{r}}, \tilde{\boldsymbol{\eta}}, \tilde{t} = \tilde{t}_0|\tilde{\mathbf{r}}_0, \tilde{\boldsymbol{\eta}}_0, \tilde{t}_0) = \delta(\tilde{\mathbf{r}}-\tilde{\mathbf{r}}_0)\delta(\tilde{\boldsymbol{\eta}}-\tilde{\boldsymbol{\eta}}_0)$. To simplify the notation, we write the conditional probability as $P(\tilde{\mathbf{r}}, \tilde{\boldsymbol{\eta}}, \tilde{t}) = P(\tilde{\mathbf{r}}, \tilde{\boldsymbol{\eta}}, \tilde{t}|\tilde{\mathbf{r}}_0, \tilde{\boldsymbol{\eta}}_0, \tilde{t}_0)$ and eventually arrive at the following Fokker-Planck

equation

$$\begin{aligned} \frac{\partial}{\partial \tilde{t}} P(\tilde{\mathbf{r}}, \tilde{\boldsymbol{\eta}}, \tilde{t}) = & -\frac{\partial}{\partial \tilde{r}_3} [\tilde{v}(\tilde{r}_3)P(\tilde{\mathbf{r}}, \tilde{\boldsymbol{\eta}}, \tilde{t})] - \sqrt{2\tilde{D}_a}\tilde{\boldsymbol{\eta}} \cdot \nabla_{\tilde{\mathbf{r}}} P(\tilde{\mathbf{r}}, \tilde{\boldsymbol{\eta}}, \tilde{t}) \\ & + \nabla_{\tilde{\mathbf{r}}}^2 [\tilde{D}(\tilde{r}_3)P(\tilde{\mathbf{r}}, \tilde{\boldsymbol{\eta}}, \tilde{t})] + \frac{1}{\tau_a} \nabla_{\tilde{\boldsymbol{\eta}}} \cdot [\tilde{\boldsymbol{\eta}}P(\tilde{\mathbf{r}}, \tilde{\boldsymbol{\eta}}, \tilde{t})] \\ & + \frac{1}{2\tau_a^2} \nabla_{\tilde{\boldsymbol{\eta}}}^2 P(\tilde{\mathbf{r}}, \tilde{\boldsymbol{\eta}}, \tilde{t}). \end{aligned} \quad (6)$$

Although Eq. (6) contains both microscopic and macroscopic scales, we are interested in the long term behavior and hence seek to extract the effective ‘‘macroscopic dynamics’’ from it, which we describe presently.

III. RESULTS

A. Method of multiple scales

The macroscopic length characterizing the heat flux is

$$L = \frac{T_m}{|\nabla T|}. \quad (7)$$

The particle scale l is such that $l \ll L$, and hence we can define a small parameter ϵ as

$$\epsilon = \frac{l}{L}. \quad (8)$$

We introduce the following dimensionless quantities

$$\begin{aligned} \boldsymbol{\eta} = \sqrt{\tau_a}\tilde{\boldsymbol{\eta}}, \quad \mathbf{r} = \frac{\tilde{\mathbf{r}}}{l}, \quad t = \frac{\tilde{t}}{\tau}, \quad v = \frac{\tilde{v}}{u}, \quad v_a = \frac{\tilde{v}_a}{v_{ac}} \\ \text{and } D = \frac{\tilde{D}}{D_c}, \end{aligned} \quad (9)$$

where $\tilde{v}_a = \sqrt{\frac{2\tilde{D}_a}{\tau_a}}$ [64], u and D_c are the characteristic values of the regelation velocity and the premelting induced diffusivity respectively. Thus Eq. (6) becomes

$$\begin{aligned} P_l \frac{\partial}{\partial t} P = & -P_e \frac{\partial}{\partial r_3} [vP] - P_a v_a \boldsymbol{\eta} \cdot \nabla_{\mathbf{r}} P + \nabla_{\mathbf{r}}^2 [DP] \\ & + P_A \nabla_{\boldsymbol{\eta}} \cdot [\boldsymbol{\eta}P] + \frac{1}{2} P_A \nabla_{\boldsymbol{\eta}}^2 P, \end{aligned} \quad (10)$$

in which the following dimensionless numbers appear;

$$P_e = \frac{ul}{D_c}, \quad P_a = \frac{v_{ac}l}{D_c}, \quad P_l = \frac{l^2}{D_c\tau} \quad \text{and} \quad P_A = \frac{l^2}{D_c\tau_a}. \quad (11)$$

We identify four characteristic time scales: $t_l^{\text{diff}} = l^2/D_c$, $t_l^{\text{adv}} = l/u$, $t_L^{\text{diff}} = L^2/D_c$ and $t_L^{\text{adv}} = L/u$ associated with microscopic (macroscopic) diffusion and advection on the particle scale l (thermal length scale L). The ratio of characteristic time for diffusion and advection is the Péclet number

$$P_e = \frac{t_l^{\text{diff}}}{t_l^{\text{adv}}} \quad \text{and} \quad P_e^L = \frac{t_L^{\text{diff}}}{t_L^{\text{adv}}}. \quad (12)$$

As a result of the external temperature gradient, our system is driven by thermal regelation, therefore advection dominates on the macroscopic scale and $P_e^L = \mathcal{O}(1/\epsilon)$, or equivalently, $t_L^{\text{adv}} = \epsilon t_L^{\text{diff}}$. However, because $P_e = \mathcal{O}(1)$ we have $t_L^{\text{adv}} = t_L^{\text{diff}}$. Thus, on the macroscopic scale, the Péclet number P_e^L is large, advection dominates, and we use the macroscopic advection time $\tau = t_L^{\text{adv}}$ as our characteristic time, leading to

$$\begin{aligned} \epsilon \frac{\partial}{\partial t} P &= -\frac{\partial}{\partial r_3} [vP] - P_a v_a \boldsymbol{\eta} \cdot \nabla_{\mathbf{r}} P + \nabla_{\mathbf{r}}^2 [DP] \\ &+ P_A \nabla_{\boldsymbol{\eta}} [\boldsymbol{\eta}P] + \frac{1}{2} P_A \nabla_{\boldsymbol{\eta}}^2 P. \end{aligned} \quad (13)$$

We introduce a dimensionless macroscopic length, $\mathbf{R} = \tilde{\mathbf{r}}/L$, and a dimensionless microscopic time, $T = \tilde{t}/t_l^{\text{adv}}$, thereby stretching the scales

$$\mathbf{r} = \frac{1}{\epsilon} \mathbf{R} \text{ and } T = \frac{1}{\epsilon} t. \quad (14)$$

Now, invoking a power series ansatz

$$P = P^0 + \epsilon P^1 + \epsilon^2 P^2, \quad (15)$$

we derive a system of equations at each order in ϵ [65–67], which are

$$\mathcal{O}(\epsilon^0) : \mathcal{L}P^0 = 0, \quad (16)$$

$$\mathcal{O}(\epsilon) : \mathcal{L}P^1 = \frac{\partial}{\partial T} P^0 + \frac{\partial}{\partial R_3} [vP^0] + P_a v_a \boldsymbol{\eta} \cdot \nabla_{\mathbf{R}} P^0 - 2\nabla_{\mathbf{r}} \cdot \nabla_{\mathbf{R}} [DP^0], \quad (17)$$

$$\begin{aligned} \mathcal{O}(\epsilon^2) : \mathcal{L}P^2 &= \frac{\partial}{\partial T} P^1 + \frac{\partial}{\partial t} P^0 + \frac{\partial}{\partial R_3} [vP^1] + P_a v_a \boldsymbol{\eta} \cdot \nabla_{\mathbf{R}} P^1 - 2\nabla_{\mathbf{r}} \cdot \nabla_{\mathbf{R}} [DP^1] \\ &- \nabla_{\mathbf{R}}^2 [DP^0], \end{aligned} \quad (18)$$

where $\mathcal{L} = \mathcal{M} + \mathcal{Q}$, with $\mathcal{M} = -\frac{\partial}{\partial r_3} v - P_a v_a \boldsymbol{\eta} \cdot \nabla_{\mathbf{r}} + \nabla_{\mathbf{r}}^2 D$, and $\mathcal{Q} = P_A \nabla_{\boldsymbol{\eta}} \cdot \boldsymbol{\eta} + \frac{P_A}{2} \nabla_{\boldsymbol{\eta}}^2$. Following [56, 68] we solve Eqs. (16)-(18). The solution of the leading order Eq. (16) is derived by making the following product ansatz

$$P^0(\mathbf{r}, \mathbf{R}, \boldsymbol{\eta}, T, t) = w(\mathbf{r}, \boldsymbol{\eta}) \rho^0(\mathbf{R}, T, t). \quad (19)$$

We integrate by parts over the microscale variables \mathbf{r} and $\boldsymbol{\eta}$, and use periodic boundary conditions to obtain the so-called weak formulation of the leading order equation [69, 70]. The existence and uniqueness of P^0 is insured by use of the Lax-Milgram theorem [69, 71], otherwise known as the solvability condition [68, 72, 73] or the Fredholm alternative [74, 75]. Thus, P^0 is constant over $P^0(\mathbf{r}, \mathbf{R}, \boldsymbol{\eta}, T, t) = P^0(\mathbf{R}, \boldsymbol{\eta}, T, t)$ and Eq. (16) becomes

$$\nabla_{\boldsymbol{\eta}} \cdot [\boldsymbol{\eta}w] + \frac{1}{2} \nabla_{\boldsymbol{\eta}}^2 w = 0. \quad (20)$$

Using the known result for a multi-dimensional Ornstein-Uhlenbeck process [76], the solution for w is given by

$$w(\eta_1, \eta_2, \eta_3) = \prod_{i=1}^3 \frac{1}{\sqrt{2\pi}} e^{-\frac{\eta_i^2}{2}}. \quad (21)$$

The solvability condition for the equation at $\mathcal{O}(\epsilon)$ is

$$\begin{aligned} \int d\mathbf{r} d\boldsymbol{\eta} \left(w \frac{\partial}{\partial T} \rho^0 + w \frac{\partial}{\partial R_3} [v\rho^0] + w P_a v_a \boldsymbol{\eta} \cdot \nabla_{\mathbf{R}} \rho^0 \right) \\ = 0, \end{aligned} \quad (22)$$

which depends on the leading order result, P^0 , from which we find that

$$\frac{\partial}{\partial T} \rho^0 = -\frac{\partial}{\partial R_3} [v\rho^0], \quad (23)$$

and Eq. (17) becomes

$$\mathcal{L}P^1 = w P_a v_a \boldsymbol{\eta} \cdot \nabla_{\mathbf{R}} \rho^0. \quad (24)$$

Now, assuming that

$$P^1 = w P_a v_a \boldsymbol{\alpha} \cdot \nabla_{\mathbf{R}} \rho^0, \quad (25)$$

we find

$$\boldsymbol{\alpha} = -\frac{1}{P_A} \boldsymbol{\eta}. \quad (26)$$

Using P^1 and the solvability condition in Eq. (18) we obtain

$$\frac{\partial}{\partial t} \rho^0 = \frac{P_a^2 v_a^2}{2P_A} \nabla_{\mathbf{R}} \rho^0 + \nabla_{\mathbf{R}}^2 [D\rho^0], \quad (27)$$

which in dimensional form is

$$\frac{\partial}{\partial \tilde{t}} \rho = -\frac{\partial}{\partial \tilde{r}_3} [\tilde{v}\rho] + \tilde{D}_a \nabla_{\tilde{\mathbf{r}}}^2 \rho + \nabla_{\tilde{\mathbf{r}}}^2 [\tilde{D}(\tilde{r}_3)\rho]. \quad (28)$$

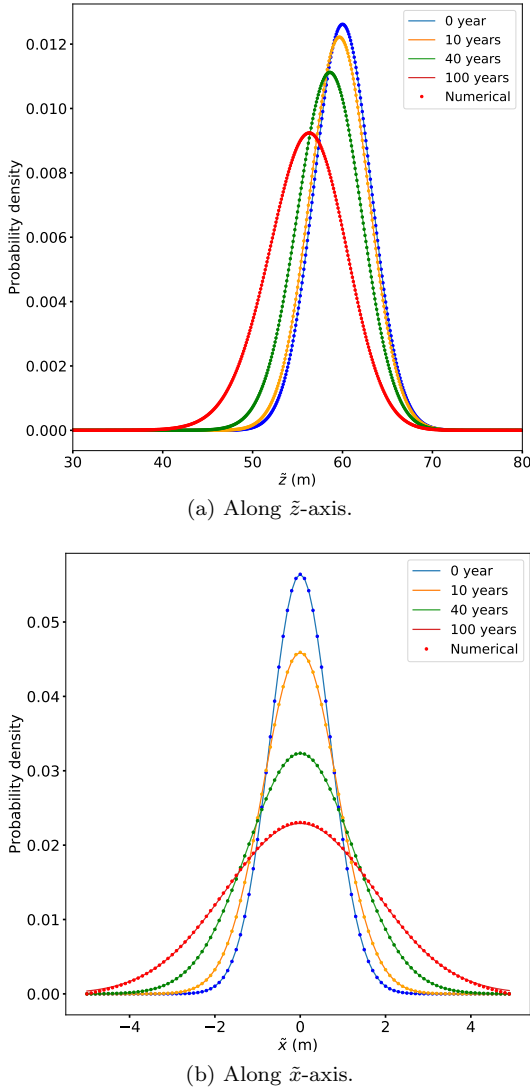


FIG. 2. Comparison between the analytic solution (solid lines), Eq. (32), and numerical solution (dots) of Eq. (29) using a finite difference method. At $\tilde{t} = 0$, the initial position of the active particle is $\tilde{z}_0 = 60\text{m}$, and the corresponding probability density function is given by Eq. (33). The evolution of the probability density function (a) Along the \tilde{z} -axis at $\tilde{x} = \tilde{y} = 0$. (b) Along the \tilde{x} -axis at $\tilde{y} = 0$ and $\tilde{z} = 59\text{m}$. The times are shown in the insets. Both figures are computed for a particle radius $R = 10^{-6}\text{m}$, with a concentration of impurities $N_i = 100\mu\text{Mm}^{-2}$, a temperature gradient $|\nabla T| = 0.1\text{Km}^{-1}$ and an active diffusivity $\tilde{D}_a = 1000\tilde{D}$.

B. Solution of the Fokker-Planck equation in the large Péclet function limit

We rewrite Eq. (28) as

$$\frac{\partial}{\partial \tilde{t}} \rho + \left[\tilde{v} - 2 \frac{\partial}{\partial \tilde{z}} \tilde{D} \right] \frac{\partial}{\partial \tilde{z}} \rho = -\rho \left(\frac{\partial}{\partial \tilde{z}} \tilde{v} + \frac{\partial^2}{\partial \tilde{z}^2} \tilde{D} \right) + \tilde{D}_{\text{eff}} \nabla^2 \rho, \quad (29)$$

where $\tilde{D}_{\text{eff}}(\tilde{z}) = \tilde{D}_a + \tilde{D}(\tilde{z})$ is the effective diffusion coefficient. As was done in [34], we define the Péclet function as

$$\text{Pe}(\tilde{z}) = \frac{\left[\tilde{v} - 2 \frac{\partial}{\partial \tilde{z}} \tilde{D} \right] L}{\tilde{D}_{\text{eff}}}, \quad (30)$$

which facilitates the solution of Eq. (29). As a reminder, L is the macroscopic thermal diffusion length scale along the \tilde{z} -direction. When Pe is large, diffusion in the \tilde{z} -direction can be neglected relative to regulation driven advection [34] and Eq. (29) becomes

$$\frac{\partial}{\partial \tilde{t}} \rho + \tilde{v} \frac{\partial}{\partial \tilde{z}} \rho = -\rho \frac{\partial}{\partial \tilde{z}} \tilde{v} + \tilde{D}_{\text{eff}} \left[\frac{\partial^2}{\partial \tilde{x}^2} \rho + \frac{\partial^2}{\partial \tilde{y}^2} \rho \right], \quad (31)$$

the solution to which is given by

$$\begin{aligned} \rho(\tilde{\mathbf{r}}, \tilde{t}) &= \frac{\tilde{z}'^3}{(\tilde{z}')^{3/4}} \exp \left(- \frac{[(\tilde{z}')^{1/4} - \tilde{z}_0]^2}{20 + 4\tilde{D}_a \tilde{t}} \right) \\ &\times \exp \left[- \frac{(\tilde{x}^2 + \tilde{y}^2)}{\left(1 + 4 \frac{\tilde{D}(\tilde{z})}{\tilde{v}(\tilde{z})} [(\tilde{z}')^{1/4} - \tilde{z}] + 4\tilde{D}_a \tilde{t} \right)} \right] \\ &\times \frac{1}{7.926\pi \left(1 + 4 \frac{\tilde{D}(\tilde{z})}{\tilde{v}(\tilde{z})} [(\tilde{z}')^{1/4} - \tilde{z}] + 4\tilde{D}_a \tilde{t} \right)}, \end{aligned} \quad (32)$$

with $\tilde{z}' = 4 \frac{A_3}{A_2} \tilde{t} + \tilde{z}^4$. Equation (32) is a consequence of the particular parameters of interest here which insure that the Péclet function in Eq. (30) is large so that, as noted above, thermal regulation dominates particle dynamics. Clearly, however, this depends on the temperature gradient, particle size and impurity concentration. Here for $R = 10^{-6}\text{m}$ the regulation induced effective diffusivity is of order $10^{-12}\text{m}^2\text{s}^{-1}$, whereas for similar sized active particles as the algae *Chlamydomonas reinhardtii* [77–79], the bacteria *Erichia coli* [80, 81] and *Pseudomonas viscosa* [81], active droplets [22, 82], and recent speed measurements of biota in ice [83, 84], we find a range of active diffusivity; $\tilde{D}_a \in [10\tilde{D}, 2000\tilde{D}]$.

Figure 2 shows the numerical solution of Eq. (29) and the analytical solution given by Eq. (32), for an active diffusivity $\tilde{D}_a = 1000\tilde{D}$. The initial position of the particle is $\tilde{z}_0 = 60\text{m}$ and the corresponding probability density function is given by

$$\rho(\tilde{\mathbf{r}}, \tilde{t} = 0) = \frac{1}{7.926\pi} \exp \left[- \frac{(\tilde{z} - \tilde{z}_0)^2}{20} - (\tilde{x}^2 + \tilde{y}^2) \right]. \quad (33)$$

Figure 2a) shows the dependence of $\rho(\tilde{\mathbf{r}}, \tilde{t})$ on the position \tilde{z} parallel to the temperature gradient, at $\tilde{x} = \tilde{y} = 0$ at different times. We observe that $\rho(\tilde{\mathbf{r}}, \tilde{t})$ spreads and displaces in the direction of higher temperatures, clearly showing the dominant influence of thermal regulation. Figure 2b) shows the dependence of $\rho(\tilde{\mathbf{r}}, \tilde{t})$ on the position \tilde{x} for $\tilde{y} = 0$ and $\tilde{z} = 59\text{m}$ at different times. Clearly

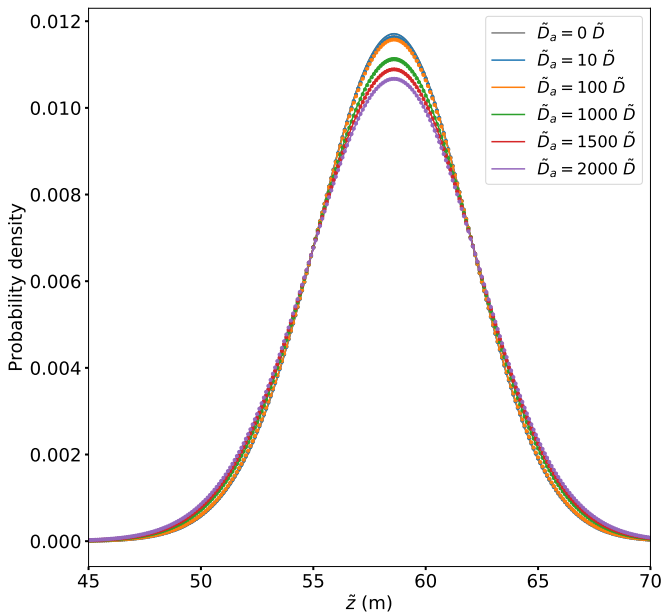


FIG. 3. The effect of the activity on the dynamics. Evolution of the probability density along the \tilde{z} -axis, computed from Eq. (32), for $\tilde{x} = \tilde{y} = 0$, initial condition $\tilde{z}_0 = 60\text{m}$ at time $\tilde{t} = 40$ years for different active diffusivities \tilde{D}_a shown in the inset. The analytic solution (solid lines), Eq. (32) is compared with numerical solution (dots), computed from Eq. (29), with $R = 10^{-6}\text{m}$, $N_i = 100\mu\text{Mm}^{-2}$ and $|\nabla T| = 0.1\text{K m}^{-1}$.

the behavior parallel to the temperature gradient is both advective and diffusive, whereas that perpendicular is diffusive, showing the competition inherent to this system.

To assess the importance of activity on the dynamics we vary the active diffusivity from low to high viz., $\tilde{D}_a \in [10\tilde{D}, 2000\tilde{D}]$. Figure 3 shows the evolution of $\rho(\tilde{\mathbf{r}}, \tilde{t} = 40\text{yr})$, along the \tilde{z} -axis, for the same particle size, impurity concentration and temperature gradient as in Fig. 2 with $\tilde{x} = \tilde{y} = 0$. The active diffusivity \tilde{D}_a affects the effective diffusion coefficient \tilde{D}_{eff} . When the activity is neglected, we recover the results from [34]. However, as the activity increases, the effective diffusion coefficient also increases. In the case when the activity becomes extremely large, the Péclet function decreases substantially and the limit of large Péclet is no longer valid. However, this behavior is unrealistic for the parameters of interest [78–81, 83, 84]. Therefore, although the effective diffusion coefficient increases, the large Péclet limit is still valid, as shown in Fig. 3. The analytic solution (solid lines), Eq. (32), compares well with numerical solutions (dots), Eq. (29). However, the increase in the diffusivity induced by the activity changes the precision of the dating method to uncertainties that should be of interest [6, 39, 41].

To gauge the effect of impurities on the dynamics, we vary N_i , from $50\mu\text{Mm}^{-2}$ to $150\mu\text{Mm}^{-2}$ and compute the evolution of the displacement along the \tilde{z} -axis, for an active diffusivity of $\tilde{D}_a = 1000\tilde{D}$. In agreement with previous work [34], because of the sensitivity of the premelted film thickness with impurity concentration, the flux of

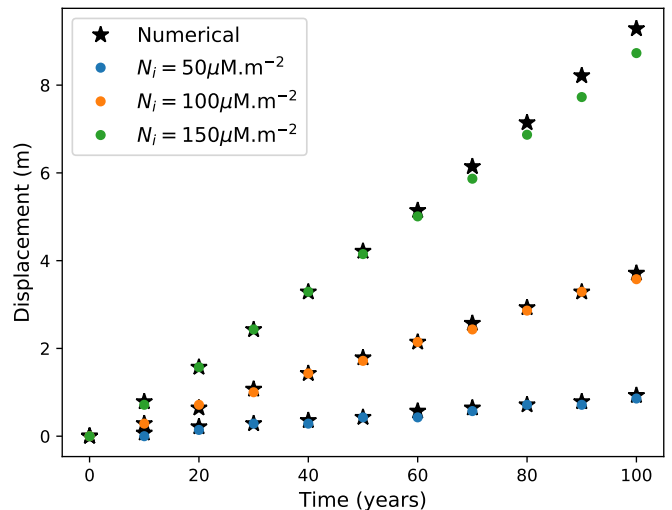


FIG. 4. The displacement dynamics along the \tilde{z} -axis, for different concentration of impurities N_i . Here, the particle radius is $R = 10^{-6}\text{m}$ and initial condition is $\tilde{z}_0 = 60\text{m}$, with a temperature gradient $|\nabla T| = 0.1\text{K m}^{-1}$ and an active diffusivity $\tilde{D}_a = 1000\tilde{D}$.

unfrozen water increases with concentration and hence so too does the regelation rate, as shown in Fig. 4. The sensitivity of the dynamics to impurities is reflected in the small discrepancy between the analytic and numerical solution for the long times and large concentrations. It is known that the presence of active particles in ice, such as bacteria or algae, and their concentrations reflects the past state of the environment [3, 85], suggesting the importance of a quantitative understanding of the role of impurities in controlling the transport mechanisms of such particles.

IV. CONCLUSION

Thermal regelation of active particles provides an interesting framework with many applications [86, 87]. Here, we have treated the dynamics of one active particle experiencing thermal regelation in three dimensions within the framework of an active Ornstein-Uhlenbeck particle. Firstly, we used a multi-scale expansion to derive the relevant Fokker-Planck equation, Eq. (32). Secondly, by taking the limit wherein thermal regelation dominated, an associated Péclet function given by Eq. (30) is large, which allows one to find an analytic solution, Eq. (29), to Eq. (32). We showed that, in the regimes of relevance to a range of particles in ice and a large range of active diffusivity, \tilde{D}_a , this limit holds, as reflected in the comparison with the numerical solution.

An important implication concerns the dating methods in ice core paleoclimatology. In particular, because of the importance of the diffusivity, our finding that this increases with activity may be reflected in dating uncertainties [39, 88]. Finally, of relevance to both ice core

dating and extremophiles is the influence impurities on the dynamics as shown in Fig. 4. By increasing the concentration of impurities the particle displacement increases substantially and hence we expect this effect to be important for both inert and living particle dynamics. Indeed, an interesting question concerns directed biolocomotion that opposes thermal regelation. Do biota “swim” against the thermo-molecular pressure gradient? How do these gradients compete with those associated with nutrients within an ice sheet [89, 90]? Finally, generalizing these questions to multiple active particles may reveal intriguing biological effects, as suggested in recent

studies of multiple passive particles [35]. The framework described here provides a starting point for generalization to address these and related questions.

ACKNOWLEDGMENTS

We acknowledge Navaneeth Marath, Marc Suñé Simon, Anthony Bonfils, Ralf Eichhorn, Sivaramakrishnan Ravichandran and Woosok Moon for helpful discussions and advice.

-
- [1] A. M. Anesio, S. Lutz, N. A. M. Chrismas, and L. G. Benning, *npj Biofilms and Microbiomes* **3**, 1 (2017).
 - [2] R. Pandey, K. Usui, R. A. Livingstone, S. A. Fischer, J. Pfaendtner, E. H. G. Backus, Y. Nagata, J. Fröhlich-Nowoisky, L. Schmäser, S. Mauri, *et al.*, *Sci. Adv.* **2**, e1501630 (2016).
 - [3] A. Abramov, T. Vishnivetskaya, and E. Rivkina, *FEMS Microbiol. Ecol.* **97**, fiae260 (2021).
 - [4] R. Margesin, F. Schinner, J.-C. Marx, and C. Gerday, *Psychrophiles: from biodiversity to biotechnology* (Springer, 2008).
 - [5] B. Stauffer, J. Flückiger, E. Wolff, and P. Barnes, *Ann. Glaciol.* **39**, 93 (2004).
 - [6] A. Royer, M. De Angelis, and J. R. Petit, *Climatic Change* **5**, 381 (1983).
 - [7] H. Wager, *Philos. Trans. R. Soc. Lond. B* **201**, 333 (1911).
 - [8] G. Gompper, R. G. Winkler, T. Speck, A. Solon, C. Nardini, F. Peruani, H. Löwen, R. Golestanian, U. B. Kaupp, L. Alvarez, *et al.*, *J. Phys. Condens. Matter* **32**, 193001 (2020).
 - [9] C. Bechinger, R. Di Leonardo, H. Löwen, C. Reichhardt, G. Volpe, and G. Volpe, *Rev. Mod. Phys.* **88**, 045006 (2016).
 - [10] C. J. Williamson, J. Cook, A. Tedstone, M. Yallop, J. McCutcheon, E. Poniecka, D. Campbell, T. Irvine-Fynn, J. McQuaid, M. Tranter, *et al.*, *Proc. Natl. Acad. Sci. USA* **117**, 5694 (2020).
 - [11] J. C. Ryan, A. Hubbard, M. Stibal, T. D. Irvine-Fynn, J. Cook, L. C. Smith, K. Cameron, and J. Box, *Nat. Commun.* **9**, 1 (2018).
 - [12] M. A. Van Leeuwe, L. Tedesco, K. R. Arrigo, P. Assmy, K. Campbell, K. M. Meiners, J. M. Rintala, V. Selz, D. N. Thomas, J. Stefels, *et al.*, *Elementa: Science of the Anthropocene* (2018).
 - [13] C. F. Aumack, A. R. Juhl, and C. Krembs, *J. Mar. Syst.* **139**, 496 (2014).
 - [14] C. A. Lindensmith, S. Rider, M. Bedrossian, J. K. Wallace, E. Serabyn, G. M. Showalter, J. W. Deming, and J. L. Nadeau, *PloS One* **11**, e0147700 (2016).
 - [15] L. Shmakova, S. Malavin, N. Iakovenko, T. Vishnivetskaya, D. Shain, M. Plewka, and E. Rivkina, *Curr. Biol.* **31**, R712 (2021).
 - [16] M. A. Mapalo, N. Robin, B. E. Boudinot, J. Ortega-Hernández, and P. Barden, *Proc. R. Soc. B* **288**, 20211760 (2021).
 - [17] J. Elgeti, R. G. Winkler, and G. Gompper, *Rep. Prog. Phys.* **78**, 056601 (2015).
 - [18] P. Romanczuk, M. Bär, W. Ebeling, B. Lindner, and L. Schimansky-Geier, *Eur. Phys. J.-Spec. Top.* **202**, 1 (2012).
 - [19] M. E. Cates, *Rep. Prog. Phys.* **75**, 042601 (2012).
 - [20] A. Ghosh and P. Fischer, *Nano Lett.* **9**, 2243 (2009).
 - [21] S. Kim, F. Qiu, S. Kim, A. Ghanbari, C. Moon, L. Zhang, B. J. Nelson, and H. Choi, *Adv. Mat.* **25**, 5863 (2013).
 - [22] C. Jin, J. Vachier, S. Bandyopadhyay, T. Macharashvili, and C. C. Maass, *Phys. Rev. E* **100**, 040601 (R) (2019).
 - [23] M. T. Madigan, J. M. Martinko, P. V. Dunlap, and D. P. Clark, *Int. Microbiol.* **11**, 65 (2008).
 - [24] J. Adler, *Science* **153**, 708 (1966).
 - [25] G. L. Hazelbauer, *Annu. Rev. Microbiol.* **66**, 285 (2012).
 - [26] J. Vachier and M. G. Mazza, *Eur. Phys. J. E* **42**, 11 (2019).
 - [27] J. Palacci, C. Cottin-Bizonne, C. Ybert, and L. Bocquet, *Phys. Rev. Lett.* **105**, 088304 (2010).
 - [28] F. Ginot, A. Solon, Y. Kafri, C. Ybert, J. Tailleur, and C. Cottin-Bizonne, *New J. Phys.* **20**, 115001 (2018).
 - [29] S. Hermann and M. Schmidt, *Soft Matter* **14**, 1614 (2018).
 - [30] J. G. Dash, A. W. Rempel, and J. S. Wettlaufer, *Rev. Mod. Phys.* **78**, 695 (2006).
 - [31] S. S. L. Peppin, M. J. Spannuth, and J. S. Wettlaufer, *J. Stat. Phys.* **134**, 701 (2009).
 - [32] J. S. Wettlaufer and M. G. Worster, *Ann. Rev. Fluid Mech.* **38**, 427 (2006).
 - [33] A. W. Rempel, J. S. Wettlaufer, and M. G. Worster, *Phys. Rev. Lett.* **87**, 088501 (2001).
 - [34] N. Marath and J. S. Wettlaufer, *Soft Matter* (2020).
 - [35] M. G. Worster, S. S. L. Peppin, and J. S. Wettlaufer, *J. Fluid Mech.* **914** (2021).
 - [36] B. Hallet, *Phil. Trans. R. Soc. A* **371**, 20120357 (2013).
 - [37] L. Liu, R. S. Sletten, B. Hallet, and E. D. Waddington, *J. Geophys. Res. Earth Surface* **123**, 1797 (2018).
 - [38] H. Hansen-Goos, E. S. Thomson, and J. S. Wettlaufer, *Planet. Space Sci.* **98**, 169 (2014).
 - [39] S. Rupper, W. F. Christensen, B. R. Bickmore, L. Burgener, L. S. Koenig, M. R. Koutnik, C. Miège, and R. R. Forster, *J. Glaciol.* **61**, 163 (2015).
 - [40] G. Baccolo, B. Delmonte, E. Di Stefano, G. Cibin, I. Crotti, M. Frezzotti, D. Hampai, Y. Iizuka, A. Marcelli, and V. Maggi, *The Cryosphere Discussions*, 1 (2021).
 - [41] L. Augustin, C. Barbante, P. R. F. Barnes, J. M. Barnola,

- M. Bigler, E. Castellano, O. Cattani, J. Chappellaz, D. Dahl-Jensen, B. Delmonte, *et al.*, *Nature* **429**, 623 (2004).
- [42] L. L. Bonilla, *Phys. Rev. E* **100**, 022601 (2019).
- [43] É. Fodor, C. Nardini, M. E. Cates, J. Tailleur, P. Visco, and F. van Wijland, *Phys. Rev. Lett.* **117**, 038103 (2016).
- [44] L. Caprini and U. M. B. Marconi, *Soft Matter* **14**, 9044 (2018).
- [45] D. Martin, J. O’Byrne, M. E. Cates, É. Fodor, C. Nardini, J. Tailleur, and F. van Wijland, *Phys. Rev. E* **103**, 032607 (2021).
- [46] L. Dabelow and R. Eichhorn, *Front. Phys.* **8**, 516 (2021).
- [47] L. Caprini, U. M. B. Marconi, and A. Puglisi, *Sci. Rep.* **9**, 1 (2019).
- [48] L. Dabelow, S. Bo, and R. Eichhorn, *Phys. Rev. X* **9**, 021009 (2019).
- [49] F. J. Sevilla, R. F. Rodríguez, and J. R. Gomez-Solano, *Phys. Rev. E* **100**, 032123 (2019).
- [50] C. Maggi, M. Paoluzzi, N. Pellicciotta, A. Lepore, L. Angelani, and R. Di Leonardo, *Phys. Rev. Lett.* **113**, 238303 (2014).
- [51] C. Maggi, M. Paoluzzi, L. Angelani, and R. Di Leonardo, *Sci. Rep.* **7**, 1 (2017).
- [52] F. Donado, R. E. Moctezuma, L. López-Flores, M. Medina-Noyola, and J. L. Arauz-Lara, *Sci. Rep.* **7**, 1 (2017).
- [53] M. Wu, J. W. Roberts, S. Kim, D. L. Koch, and M. P. DeLisa, *App. Environ. Microb.* **72**, 4987 (2006).
- [54] X. L. Wu and A. Libchaber, *Phys. Rev. Lett.* **84**, 3017 (2000).
- [55] U. M. B. Marconi, C. Maggi, and S. Melchionna, *Soft Matter* **12**, 5727 (2016).
- [56] E. Aurell, S. Bo, M. Dias, R. Eichhorn, and R. Marino, *EPL (Europhysics Letters)* **114**, 30005 (2016).
- [57] E. Aurell and S. Bo, *Phys. Rev. E* **96**, 032140 (2017).
- [58] S. Bo, S. H. Lim, and R. Eichhorn, *J. Stat. Mech.- Theory E* **2019**, 084005 (2019).
- [59] H. Chen and J. L. Thiffeault, *arXiv preprint arXiv:2006.07714* (2020).
- [60] H. Vandebroek and C. Vanderzande, *Soft Matter* **13**, 2181 (2017).
- [61] P. Romanczuk and L. Schimansky-Geier, *Phys. Rev. Lett.* **106**, 230601 (2011).
- [62] J.-F. Joanny, F. Jülicher, and J. Prost, *Phys. Rev. Lett.* **90**, 168102 (2003).
- [63] F. Peruani and L. G. Morelli, *Phys. Rev. Lett.* **99**, 010602 (2007).
- [64] L. Dabelow, S. Bo, and R. Eichhorn, *J. Stat. Mech.- Theory E* **2021**, 033216 (2021).
- [65] A. Bensoussan, J.-L. Lions, and G. Papanicolaou, *Asymptotic analysis for periodic structures*, Vol. 374 (American Mathematical Soc., 2011).
- [66] E. Sánchez-Palencia, *Lecture notes in physics* **127** (1980).
- [67] C. M. Bender and S. A. Orszag, *Advanced mathematical methods for scientists and engineers I: Asymptotic methods and perturbation theory* (Springer Science & Business Media, 2013).
- [68] G. Pavliotis and A. Stuart, *Multiscale methods: averaging and homogenization* (Springer Science & Business Media, 2008).
- [69] J.-L. Auriault, C. Boutin, and C. Geindreau, *Homogenization of coupled phenomena in heterogeneous media*, Vol. 149 (John Wiley & Sons, 2010).
- [70] “Weak Formulation of Elliptic Problems,” in *Elliptic Equations: An Introductory Course* (Birkhäuser Basel, Basel, 2009) pp. 35–42.
- [71] G. C. Hsiao and W. L. Wendland, *Boundary integral equations* (Springer, 2008).
- [72] V. V. Jikov, S. M. Kozlov, and O. A. Oleinik, *Homogenization of differential operators and integral functionals* (Springer Science & Business Media, 2012).
- [73] N. S. Bakhvalov and G. Panasenko, *Homogenisation: averaging processes in periodic media: mathematical problems in the mechanics of composite materials*, Vol. 36 (Springer Science & Business Media, 2012).
- [74] R. Kreß, *J. Differ. Equations* **25**, 216 (1977).
- [75] M. Reed, *Methods of modern mathematical physics: Functional analysis* (Elsevier, 2012).
- [76] H. Risken, in *The Fokker-Planck Equation* (Springer, 1996) pp. 63–95.
- [77] A. Fragkopoulos, J. Vachier, J. Frey, F.-M. Le Menn, M. Mazza, M. Wilczek, D. Zwicker, and O. Bäumchen, (2021).
- [78] M. Brun-Cosme-Bruny, E. Bertin, B. Coasne, P. Peyla, and S. Rafai, *J. Chem. Phys.* **150**, 104901 (2019).
- [79] K. C. Leptos, J. S. Guasto, J. P. Gollub, A. I. Pesci, and R. E. Goldstein, *Phys. Rev. Lett.* **103**, 198103 (2009).
- [80] A. Weber, M. Bahrs, Z. Alirezaeizanjani, X. Zhang, C. Beta, and V. Ziburdaev, *Front. Phys.* **7**, 148 (2019).
- [81] Y.-C. Kim, *Korean J. Chem. Eng.* **13**, 282 (1996).
- [82] C. Jin, C. Krüger, and C. C. Maass, *Proc. Nat. Acad. Sci. USA* **114**, 5089 (2017).
- [83] L. M. Olsen, P. Duarte, C. Peralta-Ferriz, H. M. Kauko, M. Johansson, I. Peeken, M. Róžańska-Pluta, A. Tatarak, J. Wiktor, M. Fernandez-Mendez, *et al.*, *Sci. Rep.* **9**, 1 (2019).
- [84] U. Oberegger, G. Flaim, and P. Colangeli, *Hydrobiologia* **847**, 2203 (2020).
- [85] N. Takeuchi, Y. Ishida, and Z. Li, *J. Earth Sci.* **22**, 431 (2011).
- [86] A. T. Fisher, K. D. Mankoff, S. M. Tulaczyk, S. W. Tyler, N. Foley, *et al.*, *Sci. Adv.* **1**, e1500093 (2015).
- [87] H. Zhang, I. Hussain, M. Brust, M. F. Butler, S. P. Rannard, and A. I. Cooper, *Nat. Mater.* **4**, 787 (2005).
- [88] T. Extier, A. Landais, C. Bréant, F. Prié, L. Bazin, G. Dreyfus, D. M. Roche, and M. Leuenberger, *Quaternary Sci. Rev.* **185**, 244 (2018).
- [89] J. L. Wadham, J. R. Hawkins, L. Tarasov, L. J. Gregoire, R. G. M. Spencer, M. Gutjahr, A. Ridgwell, and K. E. Kohfeld, *Nat. Commun.* **10**, 1 (2019).
- [90] A. T. Holland, C. J. Williamson, F. Sgouridis, A. J. Tedstone, J. McCutcheon, J. M. Cook, E. Poniecka, M. L. Yallop, M. Tranter, A. M. Anesio, *et al.*, *Biogeosciences* **16**, 3283 (2019).